A therapeutic convection–enhanced macroencapsulation device for enhancing β cell viability and insulin secretion

Kisuk Yang[a,b,c,d,e,f], Eoin D. O'Cearbhaill[a,c,g], Sophie S. Liu[a], Angela Zhou[a], Girish D. Chitnis[a,c], Allison E. Hamilos[a,c], Jun Xu[a,c], Mohan K. S. Verma[a,c], Jaime A. Giraldo[h], Yoshimasa Kudo[a], Eunjee A. Lee[a,c], Yuhan Lee[a,c], Ramona Pop[i], Robert Langer[c,e,j], Douglas A. Melton[i], Dale L. Greiner[k], and Jeffrey M. Karp[a,b,c,d,l,1]

[a]Department of Anesthesiology, Perioperative, and Pain Medicine, Brigham and Women's Hospital, Boston, MA 02115; [b]Harvard Stem Cell Institute, Cambridge, MA 02138; [c]Harvard–MIT Division of Health Sciences and Technology, Cambridge, MA 02139; [d]Proteomics Platform, Broad Institute of MIT and Harvard, Cambridge, MA 02142; [e]David H. Koch Institute for Integrative Cancer Research, Massachusetts Institute of Technology, Cambridge, MA 02142; [f]Division of Bioengineering, Incheon National University, Incheon 22012, South Korea; [g]University College Dublin Centre for Biomedical Engineering, School of Mechanical and Materials Engineering, University College Dublin, Dublin D04, Ireland; [h]Research Department, JDRF, New York, NY 10281; [i]Department of Stem Cell and Regenerative Biology, Harvard Stem Cell Institute, Harvard University, Cambridge, MA 02138; [j]Department of Chemical Engineering, Massachusetts Institute of Technology, Cambridge, MA 02142; [k]Program in Molecular Medicine, Diabetes Center of Excellence, University of Massachusetts Medical School, Worcester, MA 01655; and [l]Harvard Medical School, Boston, MA 02115

Edited by Kristi S. Anseth, University of Colorado, Boulder, CO, and approved July 22, 2021 (received for review January 21, 2021)

Islet transplantation for type 1 diabetes treatment has been limited by the need for lifelong immunosuppression regimens. This challenge has prompted the development of macroencapsulation devices (MEDs) to immunoprotect the transplanted islets. While promising, conventional MEDs are faced with insufficient transport of oxygen, glucose, and insulin because of the reliance on passive diffusion. Hence, these devices are constrained to two-dimensional, wafer-like geometries with limited loading capacity to maintain cells within a distance of passive diffusion. We hypothesized that convective nutrient transport could extend the loading capacity while also promoting cell viability, rapid glucose equilibration, and the physiological levels of insulin secretion. Here, we showed that convective transport improves nutrient delivery throughout the device and affords a three-dimensional capsule geometry that encapsulates 9.7-fold-more cells than conventional MEDs. Transplantation of a convection-enhanced MED (ceMED) containing insulin-secreting β cells into immunocompetent, hyperglycemic rats demonstrated a rapid, vascular-independent, and glucose-stimulated insulin response, resulting in early amelioration of hyperglycemia, improved glucose tolerance, and reduced fibrosis. Finally, to address potential translational barriers, we outlined future steps necessary to optimize the ceMED design for long-term efficacy and clinical utility.

type 1 diabetes | convection | macroencapsulation | stem cell–derived β cells

Diabetes mellitus currently burdens over 387 million people worldwide, of which 5 to ∼10% are accounted by patients with type 1 diabetes (T1D) (1). T1D is characterized by the immune destruction of insulin-secreting β cells and the loss of glycemic regulation. Although intensive insulin injection regimens and the use of glucose monitors have been shown to effectively regulate blood glucose, patients are still unable to meet glycemic control targets. In particular, those with severe hypoglycemic events and glycemic lability cannot be effectively stabilized with these technologies (2). In 2000, the Edmonton protocol was developed as a procedure that directly infuses pancreatic islets, isolated from cadaveric donors, into the portal vein of T1D patients. This procedure led to insulin independence in patients for a short period postinfusion (3, 4). However, poor long-term graft survival due to alloimmune and autoimmune rejections and engraftment inefficiency prevents sustained, therapeutic effects (5–7). Although immunosuppressants are coadministered with the transplanted cells to prevent graft rejection, 56% of patients experience partial to complete graft loss after 1 y, and only 10% of patients remain insulin independent after 5 y (4, 8). The majority of patients also experience complications from immunosuppression, including elevated risk of opportunistic infections and cancer (4, 8, 9). In addition, islet transplantation is burdened by a major islet donor shortage, since often two or more human pancreases are needed to achieve a sufficient number of islets (10).

The complications of immune rejection could be overcome with macroencapsulation devices (MEDs), in which glucose-sensing,

Significance

Type 1 diabetes (T1D) is characterized by the autoimmune destruction of pancreatic β cells and it burdens millions worldwide. T1D patients typically require the life-long administration of insulin or immunosuppressive agents following transplantation. A macroencapsulation device (MED) acts as a bioartificial pancreas and can immunoprotect encapsulated β cells. However, conventional MEDs suffer from limited, cell-loading capacity and slow, glucose-stimulated insulin secretion (GSIS) because of the sole reliance on diffusion. Here, we developed a convection-enhanced MED (ceMED) to afford 3D capsule geometry for maximized cell loading and faster GSIS driven by convection. Overall, we demonstrated that the ceMED significantly improves nutrient exchange that enhances cell viability and GSIS, ultimately leading to a rapid reduction of hyperglycemia.

Author contributions: K.Y., E.D.O., S.S.L., G.D.C., and J.M.K. designed research; K.Y., S.S.L., A.Z., G.D.C., J.X., and M.K.S.V. performed research; K.Y. and J.M.K. contributed new reagents/analytic tools; K.Y., E.D.O., A.Z., G.D.C., A.E.H., J.X., M.K.S.V., J.A.G., Y.K., E.A.L., Y.L., R.P., R.L., D.A.M., D.L.G., and J.M.K. analyzed data; and K.Y., E.D.O., S.S.L., A.Z., G.D.C., A.E.H., J.A.G., Y.K., D.L.G., and J.M.K. wrote the paper.

Competing interest statement: J.M.K. holds equity in Frequency Therapeutics, a company that has licensed IP generated by J.M.K that may benefit financially if the IP is further validated. J.M.K. holds equity and is a member of the scientific advisory board of Pancryos. J.M.K. has been a paid consultant and or equity holder for multiple other companies (listed here https://www.karplab.net/team/jeff-karp). The interests of J.M.K. were reviewed and are subject to a management plan overseen by his institution in accordance with its conflict-of-interest policies. R.L. is a cofounder and member of the scientific advisory board of Sigilon Therapeutics. For a list of entities with which R.L. is involved, compensated, or uncompensated, see https://www.dropbox.com/s/yc3xqb5s8s94v7x/RevLangerCOI.pdf?dl=0. D.A.M. holds equity in Vertex Pharmaceuticals and is a paid consultant for that company.

This article is a PNAS Direct Submission.

[1]To whom correspondence may be addressed. Email: jeffkarp@mit.edu.

This article contains supporting information online at https://www.pnas.org/lookup/suppl/doi:10.1073/pnas.2101258118/-/DCSupplemental.

Published September 9, 2021.

insulin-secreting cell sources like pluripotent, stem cell–derived β clusters (SC-βCs) (11), or other islet sources, are transplanted within an immune-isolating vehicle to promote cell survival and function. In MEDs, islets are housed in a single compartment that selectively permits the exchange of nutrients while obstructing host immune effectors such as cells and antibodies. Over the past few decades, MEDs have successfully restored insulin independence and normoglycemia in T1D animal models (10). However, scaling these devices for human applications has been challenging. Currently, passive diffusion-based MEDs, including Encaptra, βAir Bio-Artificial Pancreas, Cell Pouch, and MAILPAN, are being explored in phase I/II clinical trials (12–14). Nevertheless, these diffusion-based devices still suffer from limitations in the transport of glucose, insulin, and other biomolecules to the core of these devices, which compromise the survival and function of encapsulated cells. Ultimately, these devices are restricted in geometry, thickness, and cell-loading capacity.

More specifically, a significant portion of encapsulated cells become nonviable immediately after transplantation because of the lack of vascularization, which results in hypoxia and limited nutrient availability. Thus, during the initial prevascularization period, which lasts ∼14-d posttransplantation, solute exchange and insulin secretion cannot occur effectively using conventional MEDs (15–17). For this reason, many encapsulated cells prematurely lose their function and eventually die. Various strategies have been developed to expediate angiogenesis around the device, especially during the initial hypoxic period after device transplantation, to reduce cell loss. Examples include prevascularization of the device, infusion of vascular endothelial growth factor, and cotransplantation of mesenchymal stem cells (15, 18–21). In another instance, βAir Bio-Artificial Pancreas incorporated a daily refillable oxygen chamber in between two islet slabs to maintain adequate oxygen supply, but the chamber is 15- to 30-fold thicker than islet layers. Despite improvements in cell viability, these strategies still cannot guarantee adequate glucose sensing and insulin release kinetics of the islets, and they further limit the available space for cell packing (22).

To supply cells with enough nutrients, it has been suggested that the islet density of the MEDs should be set to 5 to ∼10% of the volume fraction (23). Consequently, a limited mass of islets must be placed within a large device to ensure optimal nutrient distribution. Otherwise, devices exhibit extreme cell loss. For instance, TheraCyte, which packs 70 to ∼216 islet equivalent (IEQ) in 4.5 μL or 1,000 IEQ in 40 μL volume, exhibited poor cell survival (19). The remaining cells were neither capable of restoring euglycemia in rodents (1,000 to ∼2,000 IEQ required) nor sustaining a therapeutic dosage needed for humans (∼500,000 islets) in a reasonably sized device (13, 24–26).

To overcome these nutrient delivery challenges and improve cell-loading capacity, we designed a convection-enhanced MED (ceMED) to perfuse the device continuously. We hypothesized that convective nutrient transport in ceMED would 1) deliver more nutrients compared with diffusion-based devices, 2) increase cell survival beyond the distance limit of diffusion, 3) support a three-dimensional (3D), expanded cell layer to increase the loading capacity, 4) improve glucose sensitivity and timely insulin secretion via faster biomolecule transport, and 5) show efficacy in vivo by reducing hyperglycemia before vascularization. Overall, we demonstrated that the convective motion promotes survival of insulin-secreting β cells encapsulated at high density. We also demonstrated that it effectively captures the dynamics of glucose concentrations in the transplantation site, resulting in more appropriate insulin secretion with faster on/off responses. Finally, the ceMED showed early, vascular-independent reduction in blood glucose levels in hyperglycemic rat models several days prior to the critical 14-d posttransplantation.

Results

ceMED Design. Convection-based nutrient exchange system can potentially solve many limitations of a diffusion-based system. Convection can provide a more active and faster transport of fluid, both solute and solvent, throughout the device (Fig. 1*A*). On the other hand, diffusion only provides a steady transfer of solutes along a concentration gradient at the surface of the device (24). Hence, diffusion-dependent MEDs inevitably experience cell death due to limited nutrient exchange and increased hypoxia within the inner layer of cells. To determine the limitations of diffusion-based nutrient transport in MEDs, we computationally simulated nutrient transport within a conventional device (TheraCyte) (Fig. 1*B* and *SI Appendix*, Text 1). Mass transport and the flux of oxygen, glucose, and insulin through the capsule membranes were calculated for devices of varying thickness (Fig. 1*B*). While a monolayer of islets received sufficient nutrients for survival, multilayered cells had insufficient oxygen concentration (<0.0001 mM) to support insulin secretion and cell survival at the inner layers. Only cells at the outer layer were predicted to secrete insulin in such a multilayer device. These simulations demonstrate the need for active nutrient transport systems to enable high-density cell packaging in a 3D configuration.

Thus, we designed a ceMED to provide convective nutrients through a continuous flow of fluid to the encapsulated cells (Fig. 1*C*). Our prototype ceMED features two chambers, an equilibrium chamber (EqC), which collects nutrients from surroundings, and a cell chamber (CC), which houses immunoprotected cells. The EqC is enclosed by a single-layered, semipermeable polytetrafluoroethylene (PTFE) membrane with 10 μm–sized pores, while the CC is enclosed by double-layered PTFE membranes: the inner membrane and the outer membrane with pore sizes 200 nm and 10 μm, respectively (Fig. 1 *C* and *D*). Based on immune protection strategies used by TheraCyte, the outer PTFE membrane surrounding the EqC and CC promotes angiogenesis, while the inner membrane surrounding the CC selectively allows for nutrient transport and protects against immune responses (27). The perfusate is guided via a cylindrical semipermeable hollow fiber (HF) from the EqC, where it is primed with the condition in the surrounding tissue, into the core of an expanded layer of insulin-secreting β cells, providing a continuous supply of nutrients. Specifically, a molecular weight cutoff (MWCO) of 100 kDa was used for the HF, such that it selectively passes essential nutrients, including glucose and insulin (<100 kDa), while protecting islets from small molecular effectors of the host's immune system (150 to ∼900 kDa) (*SI Appendix*, Fig. S1). By the time the perfusate has reached the CC inlet, it will be primed with a similar concentration of nutrient, as the subcutaneous interstitial tissue surrounding the implant.

Investigation of Optimal Loading Conditions and Parameters of a ceMED In Vitro. Optimal device parameters were estimated with computational models of convective transport in the prototype ceMED, which demonstrated that both glucose and oxygen transport increase as a function of flow rate. The convective transport also allowed nutrients to permeate the modeled device interior to supply islets situated beyond the diffusion limit from the membrane surfaces (Fig. 2*A* and *SI Appendix*, Text 1). The model also predicts improved insulin secretion from encapsulated cells throughout the device proportional to increased glucose transport. Specifically, the simulation data predict that, under static conditions (0 μL/h flow rate), all islets of the inner layers are hypoxic, whereas even a low flow rate (10 μL/h) modestly increases oxygen concentration for cells at the inlet, resulting in some insulin secretion. Flow rates greater than 100 μL/h are predicted to sufficiently deliver oxygen and glucose to most encapsulated cells and afford uniform insulin secretion throughout the device. In order to maintain the same device conditions in

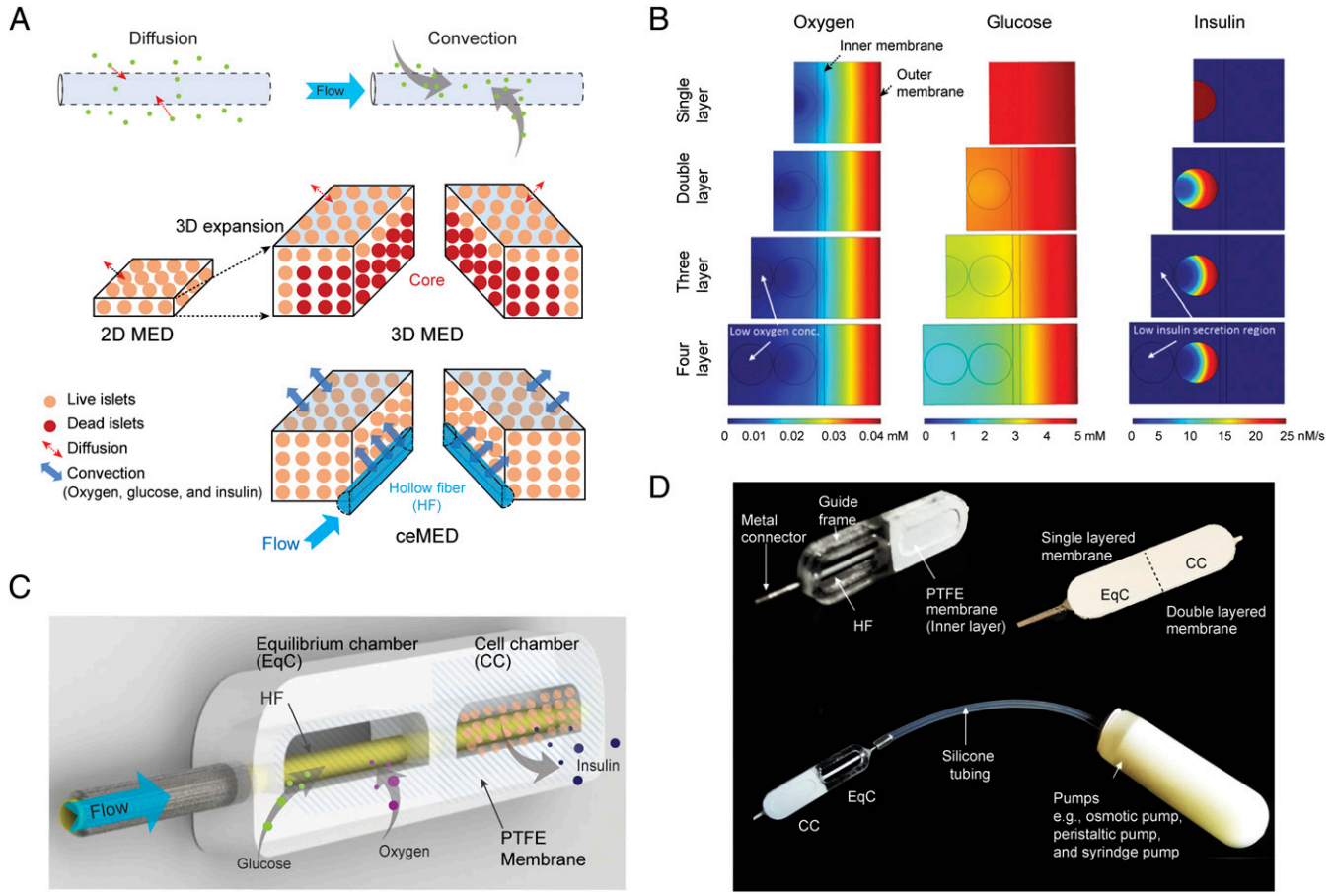

Fig. 1. Design of a ceMED for increasing mass transport, β cell viability, and insulin secretion sensitivity. (*A*) Illustration comparing diffusion-based versus convection-enhanced approaches. Expanding MEDs from a typical two-dimensional (2D) wafer static system to a 3D MED brings forth mass transport limitations and cell death. These limitations motivate the introduction of a HF in a 3D expanded MED to allow increased nutrient delivery by perfused flow in the ceMED. (*B*) Simulation showing the gradient of oxygen (millimolar), glucose concentration (millimolar), and insulin secretion rate (nanomolar per second) as a function of position inside a static macroencapsulation with multiple layers of islets. The color bars indicate the concentration of each variable. White arrows indicate the hypoxic regions in the islet due to diffusion-limited transport of the oxygen in the device. (*C*) Scheme of the ceMED, consisting of an EqC, a CC, and a connecting HF. EqC captures glucose and oxygen from the surroundings; HF transports these solutes to the encapsulated cells in the CC. Inside the CC, positive pressure facilitates flow and improved mass transport to and from the encapsulated cells. The CC is enclosed by a PTFE membrane for protection from immune attack while allowing for nutrient transfer. (*D*) Gross view of a fully assembled, transplantable ceMED and its components. The ceMED can be connected to various pump systems, exemplified here by an osmotic pump.

both no flow and flow groups, HF is also introduced into the no flow device.

To test these predicted conditions in vitro, the prototype EqC was isolated and submerged in a reservoir of 5 mM glucose, which is comparable to the physiological, basal blood glucose level (28, 29). In order to validate the effectiveness of a flow-based convection at a controlled flow rate, a syringe pump was used. The concentration of glucose present in the outflow was measured as a function of flow rate, while the EqC length was held constant at 10 mm (Fig. 2*B*). As expected, the time to reach the plateau glucose concentration at the outlet was faster at higher flow rates. A total of 100, 500, and 1,000 μL/h groups achieved plateau at 120, 60, and 30 s, respectively. However, this occurred at the expense of reduced glucose equilibration due to the insufficient residence time of the perfusate within the HF. Glucose equilibration at 100, 500, and 1,000 μL/h reached 84.2, 23.6, and 16.0% at the respective flow rates (Fig. 2*C*). To determine the relationship between EqC length (also denotes HF length) and glucose equilibration, we tested multiple EqC lengths (5, 10, and 20 mm) with a fixed flow rate of 100 μL/h. As expected, longer HFs resulted in improved equilibration, likely due to increased surface area and time for solute transfer between the fluid in the HF and the reservoir (Fig. 2*D*).

To compare the glucose concentration delivered to encapsulated cells within the CC under diffusion versus convection-enhanced conditions, the complete prototype ceMED (EqC and CC without encapsulated cells) was submerged in the same test reservoir, and fluid from the CC was collected to determine its glucose concentration (Fig. 2*E*). At plateau for the experimental group with convection (~15 min), the diffusion-based device (no flow) had 31.1% glucose equilibration, whereas perfusion at 100 μL/h resulted in 82.5% glucose equilibration (Fig. 2*F*). Perfusion at 250 μL/h flow resulted in 73.4% glucose equilibration and did not show a statistically significant difference compared with the 100 μL/h flow rate after 10 min (*SI Appendix*, Fig. S2). However, significant decrease in glucose equilibration at the 250 μL/h compared with the 100 μL/h flow rate was observed after 15 min. This difference in equilibration is presumably due to the reduced residence time for nutrient exchange in the 250-μL/h perfusion group. Altogether, our cumulative in vitro data suggest that the optimal flow rate for ceMED functionality lies within the range of 100 to ~250 μL/h.

We additionally characterized the behavior of the CC in a simulated glucose tolerance test in vitro, in which the concentration of

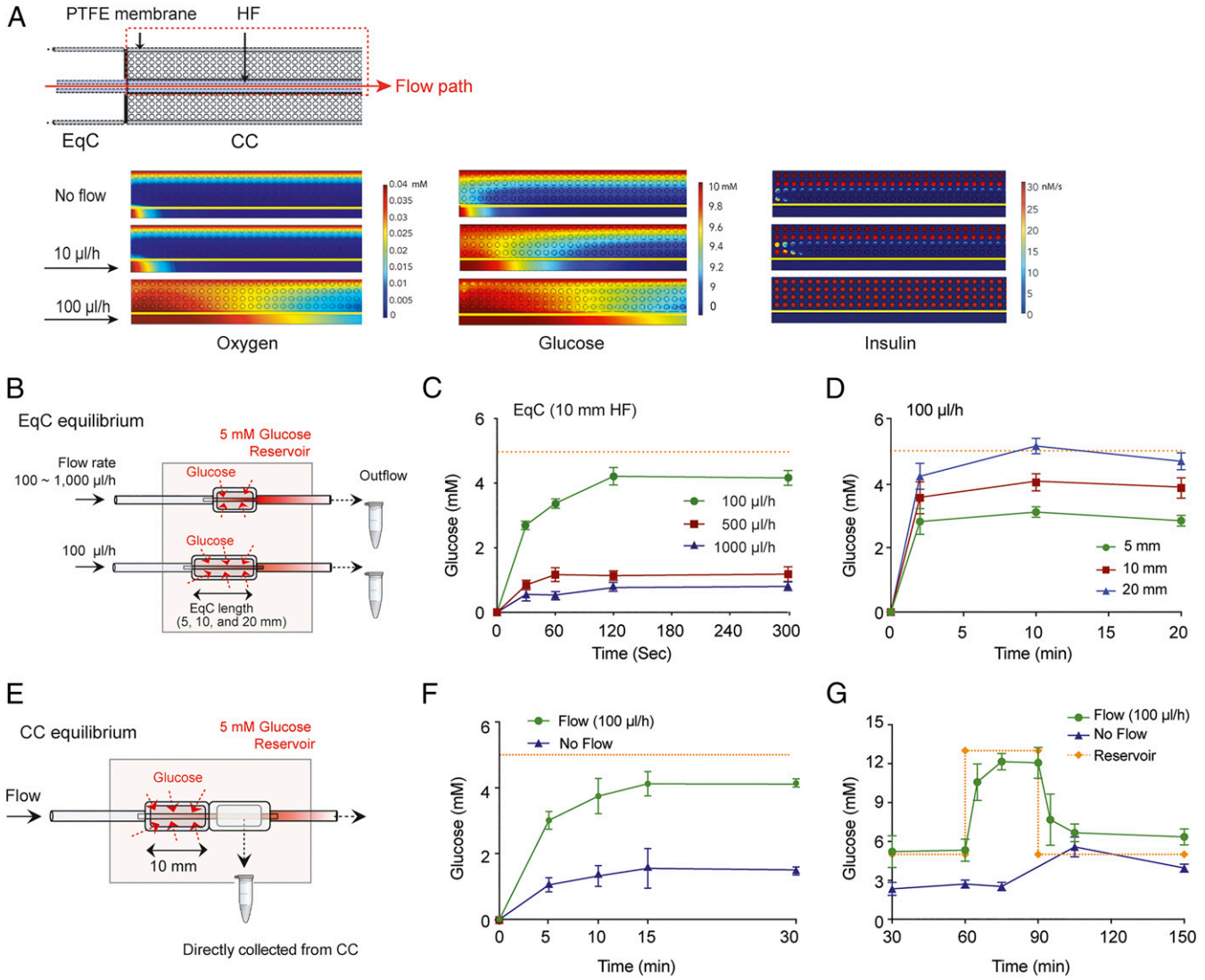

Fig. 2. In vitro optimization of the ceMED shows that lower flow rates and longer HF allows improved glucose equilibration. (*A*) COMSOL modeling of oxygen, glucose, and insulin transport in ceMED at various flow rates. The snapshot is captured at 7 min of simulation. (*B*) Illustration of experiment setup for testing the equilibration of EqC in *C* and *D*. The EqCs are submerged in 5 mM glucose solution and pumped with PBS through the HF. Outflow glucose concentration profiles are measured by Amplex red assay. (*C*) Lower flow rate allows longer residence time and improved equilibration ($n = 3$). (*D*) Longer HF length leads to more surface area and improved equilibration. Data are compiled to show the efficiency of three HF lengths (5, 10, and 20 mm) at 100 μL/h flow rate ($n = 3$). (*E*) Illustration of experimental setup for *F* and *G*. Devices are submerged in glucose solution (5 mM) and pumped with PBS through the HF. Glucose concentration profile is directly measured from the CC (with 10 mm HF) instead of the outflow. (*F*) Flow groups show increased glucose equilibration in CC compared with no flow group ($n = 3$). (*G*) Monitoring the changes in CC glucose in response to dynamic changes of glucose in the reservoir (5 to 13 to 5 mM, sequentially) ($n = 3$).

reservoir glucose was increased from basal state to postprandial blood glucose concentration (5 to 13 to 5 mM, sequentially). The postprandial state corresponds to the glucose concentration 30 to ~60 min after a meal (30). Following the 5- to 13-mM glucose transition, the ceMED glucose recovery in the 100-μL/h flow group increased rapidly during the first 5 min (at the 65-min mark, 10.6 ± 1.4 mM) and then plateaued to 93% recovery by 15 min (at the 75-min mark, 12.2 ± 0.6 mM) (Fig. 2*G*), whereas the nonperfused device recovered only 43% of reservoir glucose in 45 min (at the 105-min mark). Following the 13- to 5-mM glucose transition, the flow group experienced a rapid decrease in CC glucose concentration in the first 5 min (at the 95-min mark, 7.7 ± 1.4 mM) and then plateaued by 15 min (at the 105-min mark, 6.7 ± 0.7 mM). The observed rapid on/off response in CC glucose in the first 5 min and steadying by 15 min, following a change in reservoir glucose, is consistent with the data shown in Fig. 2*F*. These results suggest the ceMED will better recapitulate the dynamic response of the endocrine pancreas by providing a more accurate concentration of interstitial solutes to encapsulated tissue in a more timely fashion.

ceMED Shows Increased Cell Viability and Higher Insulin Secretion Activity In Vitro. To investigate the viability and functionality of encapsulated cells in vitro, ceMEDs were first loaded with MIN6 cells. MIN6 cells were chosen because of their widespread use and physiological similarity to primary human β cells, as well as for their robust glucose sensitivity and glucose-stimulated insulin secretion (GSIS) response (31, 32). We hypothesized that convection and consequent nutrient delivery through the core of the device would result in improved viability at both the outer and inner layer of cells. As expected, there was a reduction of terminal

deoxynucleotidyl transferase dUTP nick end labeling (TUNEL)–positive cells, especially surrounding the HF in the flow condition. Overall, the flow condition yielded uniform cell viability throughout the ceMED. Whereas the no flow condition yielded more cell death, indicated by increased TUNEL-positive cells surrounding the HF (Fig. 3*A*). The number of apoptotic MIN6 cells at the surface and center of the CC was significantly increased in the no flow condition compared with the flow condition (Fig. 3*B*). No significant differences in viability were observed between 10 and 20 mm EqC lengths in either condition. To see whether flow could increase the on and off rate of insulin secretion, we checked the sequential levels of insulin secretion after immersion into glucose solutions at multiple time points (Fig. 3*C*). After 10 min of 20 mM glucose challenge, the change in insulin secretion by cells in the flow group increased by ∼2.4-fold, representing a rapid "on" insulin secreting response to glucose stimulation, compared with the no flow group, which did not increase. Similarly, flow-enhanced, encapsulated cells exhibited a substantial decrease in insulin production ("off" response) by 3.6-fold, following a drop in glucose levels back to 2.8 mM, whereas the no flow device exhibited a more gradual decrease in insulin production by 2.5-fold. In addition, the cumulative GSIS index (i.e., values at 15- and 30-min post 20 mM glucose challenge divided by 15- and 30-min post 2.8 mM glucose challenge, respectively) for the flow-enhanced group showed a statistically significant, 2.5-fold increase, which is shown to be above the GSIS index range of static, cultured MIN6 cells (dashed lines) (Fig. 3*D*) (32, 33). Additionally, to further validate the cell viability of ceMED, LIVE DEAD analysis was conducted on the pluripotent SC-βCs loaded in the ceMED (*SI Appendix*, Fig. S3*A*). Similar to the MIN6 cell-loaded ceMEDs, the perfused flow also induced cell viability when loaded with SCβCs. Moreover, immunofluorescence imaging of the SC-βCs cultured for 7 d in the CC revealed that the cells in the flow group retained spherical morphology and expressed Nkx6.1 and C-peptide markers. However, the cells in the no flow group did not retain the morphology and were more scattered (*SI Appendix*, Fig. S3*B*). In addition, significantly greater GSIS indices of the encapsulated SC-βCs were

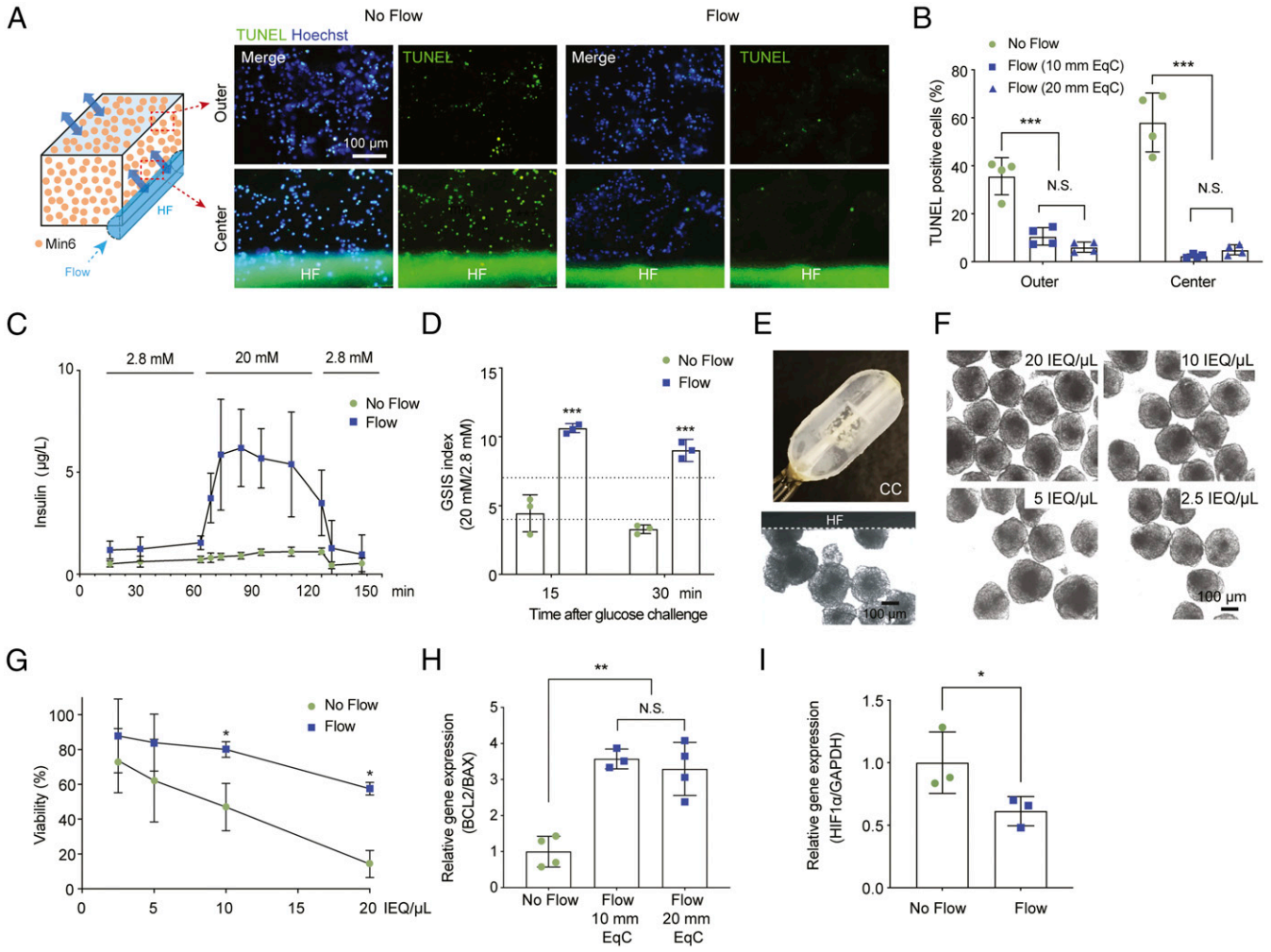

Fig. 3. ceMED shows increased viability and insulin secretion sensitivity of encapsulated cells, affording a higher loading capacity. (*A* and *B*) ceMEDs show less cell death at the outer and middle section of the device following TUNEL analysis. The lower quantification of apoptotic MIN6 cells is seen in flow groups, compared with no flow group, after 3 d in culture ($n = 4$, $^{***}P < 0.001$ versus no flow group). N.S., not significant. (*C*) Insulin secretion from MIN6 cells cultured in the ceMED shows a faster on/off rate in flow group in a GSIS test ($n = 4$). (*D*) Cumulative GSIS indices from the MIN6 cells taken at 15 and 30 min are increased in the flow group. Dashed lines indicate the GSIS index range for static MIN6 cells ($n = 3$, $^{***}P < 0.001$ versus no flow group). (*E*) Gross morphology of SC-βCs embedded in the CC. (*F* and *G*) Optimization of the loading capacity of SC-βCs in the device (2.5 to ∼20 IEQ/μL). Perfused flow allows the loading of higher cell density compared with no flow group ($n = 3$, $^{*}P < 0.05$, versus no flow group). (*H*) Gene expression of anti-apoptotic (BCL2) and proapoptotic (BAX) marker (normalized to GAPDH) of SC-βCs cultured for 2 d in ceMED. The ratio of BCL2/BAX is higher in flow group versus no flow group ($n = 3$, $^{**}P < 0.01$ versus no flow group). (*I*) HIF-1α expression of SC-βCs cultured at day 1 in the ceMED ($n = 3$, $^{*}P < 0.05$ versus no flow group).

observed in the flow groups compared with the no flow group. Also, there was no significant difference in GSIS indices between the 100- and 250-μL/h flow groups (*SI Appendix*, Fig. S3*C*). This observation further supports the earlier claim that there exists a range for optimal flow conditions between 100 to ∼250 μL/h. Altogether, perfusion of the ceMED supports overall increased viability throughout the capsule thickness, and the 3D geometry allows for highly increased cell capacity compared with no flow conditions. Moreover, convection also enhanced glucose sensing and insulin release kinetics, as well as total insulin delivered from the device after glucose stimulation.

ceMED Supports Viability of SC-βCs at an Increased Loading Capacity. Next, we sought to explore the loading capacity of the ceMED with SC-βCs, a more clinically relevant cell source. In the SC-βC protocol, SC-βCs grow in 3D clusters, of which ∼30% are β cells that have the ability to secrete insulin in response to glucose (11). The cell morphology of SC-βCs was not visibly affected after loading into the CC (Fig. 3*E*). Moreover, SC-βCs were suspended in growth factor–reduced Matrigel and injected into the CC. Matrigel was used for homogenous cell distribution, the prevention of aggregates, and shear stress reduction during loading (*SI Appendix*, Fig. S4*A*). We also investigated cell loading into the ceMED with alginate hydrogel, since alginate microspheres are commonly used for islet encapsulation (34). The ratios of expression of the anti-apoptotic marker BCL2 and the proapoptotic marker BAX (BCL/BAX) showed no significant difference between the Matrigel-embedded and the alginate-embedded cells (*SI Appendix*, Fig. S4*B*). To determine the optimal packing density for viability, SC-βCs were loaded into the CC at multiple densities of IEQs (20, 10, 5, and 2.5 IEQ/μL) (Fig. 3*F*). Their viability was compared with the encapsulated cells without perfusion. The percentage of viable cells was determined by alamarBlue assay and normalized to a control population of SC-βCs in suspension culture. After 2 d in culture, the flow-enhanced group, perfused with phosphate-buffered saline (PBS) at 100 μL/h, was loaded with 10 to ∼20 IEQ/μL and maintained significantly higher numbers of viable SC-βCs compared with the no flow condition (10 IEQ/μL: flow 81.0 ± 4.5% and no flow 47.0 ± 13.6%; 20 IEQ/μL: flow 57.5 ± 3.6% and no flow 7.8 ± 7.8%) (Fig. 3*G*). The BCL/BAX ratios further suggest enhanced viability for the flow conditions compared with no flow condition (Fig. 3*H*). However, no significant difference in viability was observed between 10- versus 20-mm long EqC. Next, to assess the sole contribution of EqC on the cell viability (decoupled from surface diffusion), we first detached the EqC from the CC. An SC-βC–containing CC was submerged in PBS. The CC was provided with either no flow, primed perfusate from an EqC, or direct infusion of culture media (*SI Appendix*, Fig. S5 *A* and *B*). When an EqC was introduced into the circuit, it provided flow-enhanced equilibration and conduced the primed PBS to the cells in CC. Subsequently, the addition of EqC resulted in a high numbers of live cells and a BCL/BAX ratio which is comparable to that of the positive control (direct perfusion of culture media into the CC), suggesting the importance of the EqC in improving SC-βC viability (*SI Appendix*, Fig. S5 *C* and *D*). Furthermore, we found that the level of hypoxia-induced factor-1α (HIF-1α) expression in the flow-enhanced group was lower than those in the no flow group (Fig. 3*I*). The HIF-1α expression is induced by low-oxygen concentrations and can modulate diverse signaling pathways involved in β cell apoptosis (35).

Glucose Equilibration across HF in Subcutaneously Transplanted ceMED. To examine glucose transport and equilibration under in vivo conditions, EqC was implanted in the subcutaneous space of nondiabetic Lewis rats using a swivel-based tether in vivo infusion setup (Fig. 4*A* and *SI Appendix*, Fig. S6 and Text 2). After surgical wound healing, to investigate whether bidirectional transport could occur across the HF, high- (20 mM) and low- (2 mM) glucose concentrations were perfused through the HF. The HF outflow was collected and analyzed for glucose concentration in comparison with blood glucose. Inflow concentrations of 20 and 2 mM in PBS were chosen to clearly visualize bidirectional transport using the largest possible range between satiated and starved glucose dynamics. Here, PBS was used as a perfusate because of its clinical uses and ability to maintain a constant pH. The initial target flow rate of 100 μL/h proved ineffective at transporting the fluid through the significantly longer length of tubing required. Thus, we sought to reestablish the optimal in vivo flow rate, starting at 250 μL/h in vivo (250, 500, and 1,000 μL/h) (Fig. 4*A*). When 20 mM glucose was infused, outflow glucose approached a concentration near normal blood glucose (5 to ∼6 mM) with decreasing flow rate, suggesting that inflow glucose equilibrated with interstitial fluid (ISF) glucose. Among the groups, 250 μL/h flow rate showed the best equilibration, which is consistent with our earlier in vitro data (Fig. 2*C* and *SI Appendix*, Fig. S2). From here on, 250 μL/h flow rate was used for the in vivo assessments.

When 2 mM glucose was infused, the outflow initially rose to equilibrate ISF concentrations (Fig. 4*B*). After 90 min, in which glucose was completely equilibrated between the EqC and ISF, we artificially increased the glucose level in the rats by performing intraperitoneal (IP) injection of glucose (2 g/kg). IP injections in the rat immediately raised its blood glucose level to up to 12 mM, which returned to normal within 40 min, with peak concentration around 30-min post–IP injection (red line). The outflow glucose (blue line) manifested a similar tendency as ISF glucose dynamics in response to blood glucose fluctuations. Together, the two experiments revealed that transport of solutes occurs across the HF in vivo in the presence of a gradient between ISF and perfused solution.

In order to provide an equilibration region for both the inflow of glucose and the outflow of insulin, the ceMED was modified with an additional EqC (Fig. 4*C*). In the CC, insulin produced by the ceMED can be released both through the membrane by diffusion and through the outflow by convection. For in vivo study, the outflow needed to be removed from the animal to prevent edema in the subcutaneous transplant site. However, by removing the outflow fluid, a large proportion of the released insulin would also be washed out and wasted. To circumvent this problem, a second EqC (i.e., insulin chamber) was added after the CC to allow the convection-enhanced release of insulin from the perfusate into surrounding tissue before it leaves the animal's body. In vitro pilot study was performed to evaluate the feasibility of this dual-EqC ceMED by comparing the performance between single EqC versus dual EqC. The dual-EqC device demonstrated substantial solute release from the second EqC while removing the outflow (*SI Appendix*, Fig. S7).

Increased Cell Viability with Convection in Subcutaneously Transplanted ceMED. Prior to testing the in vivo viability of cells encapsulated in the ceMED, an in vitro pilot study was first conducted using a cell-loaded ceMED. Cell survival was assessed under a hypoxic condition, which is to be expected at a subcutaneous transplantation site (*SI Appendix*, Fig. S8). The hypoxia condition was set at 6% oxygen, which is equivalent to the partial pressure of oxygen (40 to ∼60 mmHg) in the subcutaneous space (36). MIN6 cells were loaded at 10 IEQ/μL for all groups. The cell viability was significantly diminished under hypoxia if perfused flow was not provided. However, when the flow (250 μL/h) was provided, the cell viability was maintained and showed no significant difference between the hypoxic and normoxic condition. These results demonstrate that the cells loaded in the dual-EqC ceMED at 10 IEQ/μL, which was determined to be the optimal cell-loading capacity in earlier in vitro experiments, can also survive and be accommodated under a mildly hypoxic, subcutaneous-mimicking condition if convection is supplied.

Next, ceMED devices loaded with SC-βCs were transplanted into the subcutaneous site of Lewis rats (*SI Appendix*, Text 3).

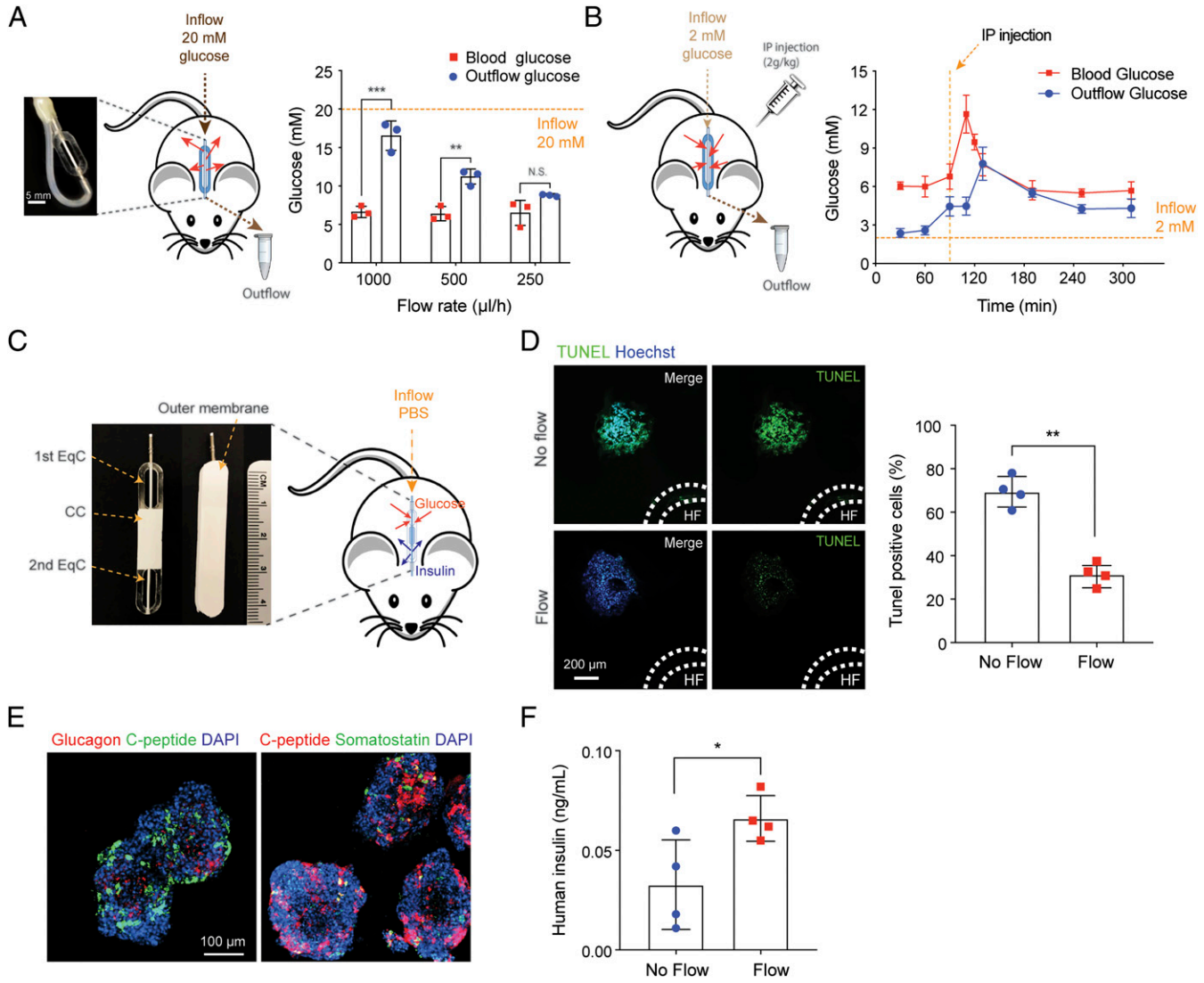

Fig. 4. Subcutaneously transplanted EqC demonstrates equilibration with interstitial glucose, resulting in increased cell viability in vivo. (*A*) Subcutaneously implanted EqC shows that an inflow of highly concentrated glucose (20 mM) through the HF can be transported out and into the ISF. The resulting outflow has glucose concentration more closely equilibrated with blood glucose. In determining the optimal flow rate for in vivo studies, lower flow rates (250 μL/h) show better equilibration ($n = 3$ rats, $^{**}P < 0.01$, $^{***}P < 0.001$ between blood and outflow glucose). (*B*) Glucose can also be transported into the HF when ISF glucose concentration (spiked with 2 g/kg IP glucose injection) is higher than the inflow concentration (2 mM) through the HF. EqC shows a timely equilibration at the 250 μL/h flow rate ($n = 3$ rats). (*C*) For in vivo transplantation, a ceMED with dual EqC is designed: The first EqC detects changes in glucose in surrounding tissues, and the second EqC allows insulin release into surrounding tissues. (*D*) Representative images and quantification of TUNEL-positive cells show that SC-βCs embedded in alginate gel in ceMEDs have higher viability compared with no flow group at 14-d posttransplantation ($n = 4$ rats, $^{**}P < 0.01$ versus no flow group). (*E*) SC-βCs retrieved from the core (near the HF) of a CC in the flow group express key endocrine markers (C-peptide, glucagon, and somatostatin) after extraction from the subcutaneous site of the rat at 7-d posttransplantation. (*F*) SC-βCs explanted from devices at 14 d posttransplantation show higher human insulin secretion in flow group ($n = 4$ rats, $^{*}P < 0.05$ versus no flow group).

Following 14-d posttransplantation, the surface of the devices showed a high density of blood vessels surrounding the outer PTFE membrane (*SI Appendix*, Fig. S9). This result is consistent with previous finding in the literature (37). The flow-enhanced devices sustained a higher viability of SC-βCs than nonflow-infused devices, as demonstrated by decreased TUNEL-positive cells (flow: 31.4 ± 5.2% and no flow: 70.0 ± 7.0%) (Fig. 4*D*). The SC-βCs retrieved from the transplantation site were shown to express key endocrine markers, including C-peptide, glucagon, and somatostatin (Fig. 4*E*). Improved function was demonstrated by significantly higher levels of human insulin compared with the no flow group (Fig. 4*F*). Overall, it was validated that the device could effectively interact with surrounding ISF and equilibrate dynamic glucose changes. Furthermore, the device could establish extensive angiogenesis and maintain cell viability, particularly in layers near the HF.

Transplantation of Glucose-sensing, Insulin-secreting Cells within the ceMED to Restore Glycemic Control. We investigated the short-term efficacy of the ceMED in supporting the viability and function of immune-isolated, glucose-sensing, and insulin-secreting cells, particularly during the prevascular 14-d period, in a chemically induced, hyperglycemic animal model. First, MIN6 cells (1.2×10^7 cells/kg, assuming 1,500 cells = 1 IEQ) embedded in an alginate hydrogel were loaded into the device at a seeding density similar to that of previously reported macroencapsulation studies, 6,500 to ~8,600 IEQ/kg (22, 36). Then the device was transplanted into the subcutaneous space of streptozotocin (STZ)-induced, immunocompetent

Lewis rats. Throughout the study, the control group did not receive infusion, while the flow group underwent perfusion with PBS at the flow rate of 250 μL/h. In the flow group, blood glucose began to decrease as early as 2-d posttransplantation and reached near normoglycemia by day 5. This result demonstrates that the flow system may promote early cell survival and insulin secretion from the ceMED, even before vascularization takes place (14-d posttransplantation). The flow group showed the continued reduction of hyperglycemia with a lower mean nonfasting blood glucose of 187.0 ± 32.9 mg/dL, compared with the no flow group (453.8 ± 57.6 mg/dL) at 25-d posttransplantation (flow: 198.2 ± 21.3 mg/dL and no flow: 495.5 ± 44.8 mg/dL at 30-d posttransplantation, Fig. 5*A*).

After transplantation, IP glucose tolerance test (IPGTT) was performed on day 14, following overnight fasting. The ceMED group showed enhanced glucose tolerance approaching near normal glycemic level (Fig. 5 *B* and *C*). Between the time of IP injection (30 min) and the time of peak blood glucose concentration (60 min), the untreated control (no device group) and transplanted rats with no flow group exhibited a steeper rise in blood glucose concentration (Δ = 234 ± 32.9 mg/dL and Δ = 208 ± 38.4 mg/dL), compared with the ceMED with flow group (Δ = 193.7 ± 11.9 mg/dL). From the time of peak blood glucose (60 to 90 min), the flow group showed improved clearance of IP-injected glucose with a greater decrease in blood glucose (Δ = −128 ± 21.3 mg/dL), compared with no flow and no device groups (Δ = −62.0 ± 46.0 mg/dL and Δ = −23.0 ± 15.7 mg/dL) (Fig. 5*C*). These results also suggest that the ceMED generates less pronounced fluctuations in blood glucose concentrations.

To check human insulin secretion, primary human islets (8,000 IEQ/kg) were loaded into the device. Similar to the MIN6 cell study, the flow group showed more effective reduction of hyperglycemia by 2-d posttransplantation. To clarify the effect of perfused flow, the syringe pump was stopped 18 d after transplantation. Interestingly, when flow was stopped in ceMED transplanted rats, blood glucose increased from 277 ± 44.1 (day 17) to 449.0 ± 134.2 (day 24) (Fig. 5*D*). Of note, the increase in blood glucose level was observed, despite the vascular formation at 14-d posttransplantation. Without convection, the blood vessels only support diffusion-based nutrient exchange at the surface of the ceMED device. We believe that the increase in blood glucose concentration after stopping the flow further emphasizes the importance of convection-based nutrient transport to support cell viability and function throughout the CC.

IPGTT was also conducted on rats transplanted with primary human islets loaded in ceMED. Like MIN6 cells, primary human islet loaded in ceMED also demonstrated reduced blood glucose fluctuation after IP injection (*SI Appendix*, Fig. S10 *A* and *B*). Importantly, a 3.9-fold increase in human insulin in the flow group indicates that glucose reduction is regulated by insulin specifically produced by the transplanted primary human islets (*SI Appendix*, Fig. S10*C*). Furthermore, immunofluorescence imaging of the retrieved primary human islets revealed that cells in the flow group retained spherical morphology and expressed C-peptide and glucagon markers. On the other hand, the cells retrieved from the no flow group did not appear to retain this morphology (Fig. 5*E*). These data suggest that the perfused flow is essential in releasing insulin from the insulin-secreting cells (C-peptide$^+$) in the islets within the ceMED for maintaining their morphology and reducing blood glucose levels.

An interesting observation made from the in vivo study is that infused devices (flow group) elicited a lower fibrotic response on the retrieved PTFE membrane when compared with the static group (no flow). This was demonstrated by the decreased macrophage (CD68) and fibrotic markers such as smooth muscle cell–α (SMC-α) and collagen type I (ColI) (Fig. 5*F*). In order to accommodate the sectioning process for histological staining, we developed a polydimethylsiloxane-based device (*SI Appendix*, Fig. S11). Histological staining of the fibrotic tissue adjacent to the CC membrane also showed that infused ceMEDs developed less fibrotic tissue around the membrane (mean thickness 321.0 ± 78.6 μm) compared with the static group (mean thickness 548.2 ± 166.5 μm) (Fig. 5 *G* and *H*). The data presented here indicates that convection through the ceMED may contribute to decreased fibrotic deposition.

Discussion

In this study, the glucose-sensing, insulin-secreting, and cell-loaded ceMED, as with many other cell therapies, provides unique advantages over conventional insulin pumps in that it acts as a biological glucose sensor that intrinsically monitors glycemic levels, produces insulin indefinitely, and secretes it on demand as needed. While we primarily presented a proof of concept of the ceMED, we also demonstrated the successful encapsulation of multiple types of glucose-sensing, insulin-secreting cell sources. In addition, convection effectively enhanced the survival and insulin-secreting function of these cells in vivo. Moreover, we have shown that perfusion in the ceMED through a HF can compensate for the delay in vascularization after transplantation. This allows the device to sustain cell viability and start to decrease blood glucose level as early as 2-d posttransplantation.

An additional benefit of external perfusion is that it avoids complications such as blood clotting and thrombosis that may arise with intravascular–encapsulation devices (26). As opposed to most static diffusion devices, the ceMED can be transplanted into the less vascularized subcutaneous site, which requires a less invasive implantation surgery. Static devices are usually limited to transplantation sites with dense vascularization such as the peritoneal cavity (38) or omentum (39). These sites are characteristically small, invasive to accommodate large-sized capsules, and highly dependent on hemocompatibility (26). Static devices also have a suggested maximum loading density of 5 to ∼10% of the total device volume in order to ensure adequate nutrient distribution, whereas the ceMED can load cells to 17.7% of the total volume (10 IEQ/μL [maximum: 56.6 IEQ/μL, assuming 150-μm diametric islets]), while sustaining islet insulin secretion and viability in vivo. The ceMED can accommodate a 9.7-fold higher cell capacity compared with TheraCyte ([ceMED: 1,621 IEQ/cm^2, dimension of dual membrane surface] versus TheraCyte [40 μL]: 167 IEQ/cm^2) (24, 35). The increased cell-loading capacity, under convection, suggests that the ceMED can maintain a smaller device size to achieve the same therapeutic effect with a less invasive transplantation.

Overall, the first-generation ceMED in this study provides a proof-of-concept validation of the perfused flow approach by demonstrating 1) enhanced nutrient transport, 2) increased cell-loading capacity and survival, 3) support for 3D expanded layered cells, 4) improved GSIS kinetics, and 5) immediate, vascular-independent amelioration of hyperglycemia in vivo. However, it is also important to recognize the key limitations of this study. Because of a number of experimental constraints, the specific prototype ceMED that we developed could not be tested for full amelioration of hyperglycemia to normoglycemia, sustaining long-term glucose regulation (several months posttransplantation). To address these constraints, there are a few barriers that must be overcome, for which we propose the following approaches: 1) fabricating next-generation ceMED device to increase cell-loading capacity and optimize dimensions, 2) replacing the syringe pump with an implantable pump for long-term generation of convective transport, and 3) using or developing more robust glucose-sensing, insulin-secreting cell source suitable for clinical applications. Additionally, understanding the immune and fibrotic longitudinal response after device transplantation can also be useful for extending the service life of ceMED.

One approach to achieve long-term normoglycemia for clinical translation includes increasing the size of the device to support sustained cell survival. Specifically, scaling up for clinical applications (500,000 islets) requires efforts in not only providing

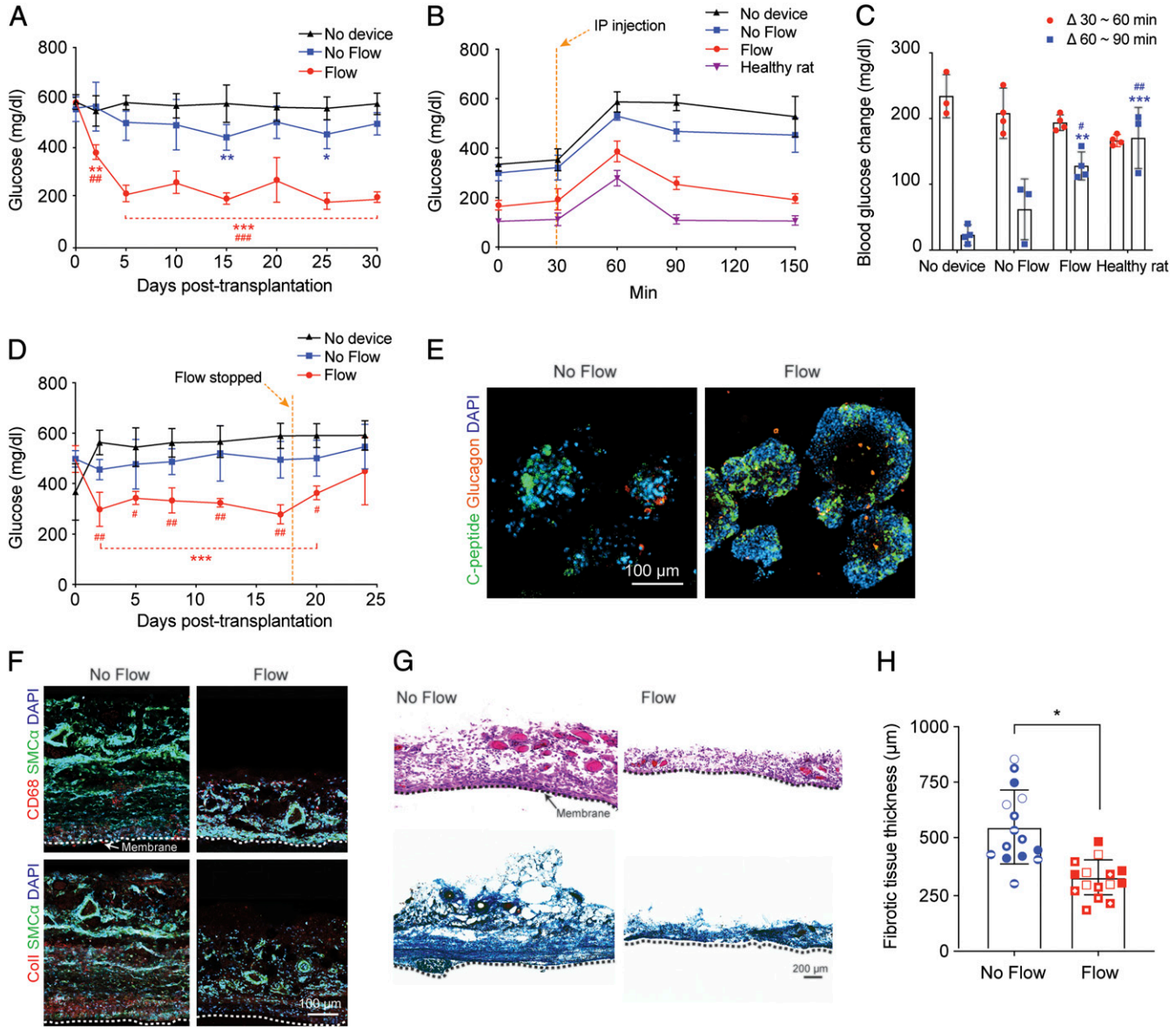

Fig. 5. Subcutaneously transplanted ceMED generates improved hyperglycemia reversal and lower fibrotic response in vivo. (*A*) Blood glucose levels decrease at day 2 in the flow group in STZ-induced, immunocompetent Lewis rat and continue to 30-d posttransplantation. The ceMED is loaded with MIN6 cells (1.2×10^7 cells/kg, $n = 3$ to ~4 rats, $^{*}P < 0.05$, $^{**}P < 0.01$, $^{***}P < 0.001$ versus no device, $^{\#\#}P < 0.01$, and $^{\#\#\#}P < 0.001$ versus no flow). (*B* and *C*) Rats in the flow group show less fluctuation and better restoration in glucose concentrations in response to IPGTT, compared with no flow and no device groups ($n = 3$ to ~4 rats, $^{**}P < 0.01$, $^{***}P < 0.001$ versus no device, $^{\#}P < 0.05$, and $^{\#\#}P < 0.01$ versus no flow). (*D*) Primary human islets in the flow group show continuous reduction in nonfasting glucose level after transplantation. When the flow is stopped, an increase in blood glucose is observed ($n = 4$ rats, $^{***}P < 0.001$ versus no device, $^{\#}P < 0.05$, and $^{\#\#}P < 0.01$ versus no flow). (*E*) Representative images showing that primary human islets embedded in alginate gel, retrieved from the core of a CC, express C-peptide and glucagon, as seen by immunofluorescence staining. (*F*) Immunofluorescence staining shows macrophage (CD68) and fibrosis markers (SMC-α and Coll) on the surface of ceMED. (*G*) Representative images of histological staining (*Top*: H&E and *Bottom*: Masson's trichrome staining) of a ceMED membrane extracted from the transplantation site show less fibrosis in the flow group. (*H*) Quantification of the fibrotic tissue thickness surrounding ceMED membrane shows decreased thickness of fibrosis in the flow group (58.6% versus no flow group) (total of 15 images from four rats [four devices] combined; different datapoint patterns used for each animal result, $^{*}P < 0.05$ versus no flow).

convection-based transfer but also by forming a loading space with maximized surface area to volume ratios. Exploring structural modifications such as folding (40) or coiling may potentially provide a solution for high surface area and compact geometries tailored for clinical application. In the current ceMED, the EqC structure is similar to the CC. However, the EqC may become more compact in next-generation ceMED (e.g., by removing guide frames) to improve the overall cell-loading capacity.

In addition to scaling up the cell-loading capacity, optimization of the perfused flow system will be necessary for long-term function and efficacy. Currently, our short-term in vivo transplantation study showed that the flow-based convention system is crucial for the survival and functionality of islets in the prevascular phase; however, a one-way fluid flow system demonstrates barriers for long-term translation. To eliminate the need for an external pump or the combination of an internal pump with a reservoir that needs periodic replenishment, a closed-loop recirculation system is important for next-generation development. Also, the long tubing and animal movements made long-term experiments difficult when using the syringe pump-mediated flow system. Because

of this, ceMED functionality assessment in vivo was stopped at 30-d posttransplantation. Furthermore, the long tubing used in our infusion system could contribute to the delay in outflow glucose concentration, which prevented the complete normoglycemia to be achieved in animal studies. Hence, the examination of long-term ceMED functionality using a closed loop pump system will be a focus of future work (*SI Appendix*, Fig. S12 and Text 4).

Finally, identifying the ideal β cell sources for long-term in vivo experimentation and clinical use is another point to be addressed. SC-βCs represent useful cell source for in vivo ceMED validations, especially considering their clinical potential. However, limitations exist with validating ceMED using SC-βCs. SC-βCs are unable to secrete insulin until 2-wk posttransplantation because of the time needed to mature into fully functional, insulin-secreting β cells in vivo (11). This limitation holds true regardless of convention or vascularization status. Thus, we plan to explore cell sources that demonstrate full functionality prior to transplantation and are also suitable for clinical translation. Improving methods to differentiate progenitor cells into fully functional SC-βCs should improve functionality.

In addition, although it was interesting to observe that the thickness of fibrosis on the surface of the ceMED was significantly decreased while convection was in place, long-term immune and fibrotic responses need to be explored. As with most implanted biomaterials and devices, foreign body response (FBR) establishes around the ceMED within weeks after transplantation (41). It may be possible that the no flow group housed more apoptotic cells because of the lack of nutrient transfer and internal hypoxia. Thus, more apoptotic cell antigens and inflammatory signals may have traversed the device membrane and attracted phagocytes to the nearby tissue (42, 43). Furthermore, as postulated by other studies exploring the effect of mechanical perturbation for reducing FBR (44), the mechanical movement of fluid flow may have decreased the FBR surrounding our device. In this study, we chose to study fibrosis development after 14 d of transplantation, according to previous studies (44, 45). Initially, posttransplantation FBR may not be as problematic because convection alone can facilitate ceMED functionality before vascularization. However, FBR may be a barrier over the long term once vascularization is replaced by extensive fibrosis. The progression of FBR may hinder glucose sensing and insulin secretion. Hence, in the future, we will investigate the mechanism by which flow reduces FBR and whether this is sustainable. We will also attempt to fully understand the series of immune events and effects that impact long-term device performance. Future studies to introduce flow as a general principle for reducing FBR in implants may also be desirable. To achieve the long-term and self-mediated suppression of inflammation, immune activity, and fibrosis around the device, multiple strategies may be explored. For example, we may consider engineering β cells or other accessory cells to secrete immunomodulatory factors and microfabricating membranes to achieve precise pore size control. Alternatively, use of the long-term, controlled release of antifibrotic drugs may be explored in overcoming the challenges associated with FBR as well (45).

Overall, ceMED demonstrated enhanced cell viability and significant reduction in blood glucose with minimal delay following transplantation in a T1D rat model. These results illuminate significant advantages over diffusion-based devices. Therefore, encapsulation coupled with the convection-aided design represents a potentially viable approach to enhance the success of β cell replacement therapies to treat T1D.

Materials and Methods

COMSOL Simulation. Prior to in vitro experimentation, computational modeling was performed using COMSOL to first predict the minimum flow rate required to maintain islet survival and function. Detailed rationale and setup of the COMSOL simulation are explained in *SI Appendix*, Text 1.

Cell Culture. The SC-βCs at stage 6 d 15 to ~25 were generously provided by Professor Douglas Melton, Harvard University, Cambridge, MA and maintained in 30 mL spinner flasks (a type of single-use bioreactor, ABLE Biott) under a previously published protocol (11). Primary human islets were obtained from Prodo Laboratories, Aliso Viejo, CA under guidelines approved by the Brigham and Women's Hospital Biosafety Registrations. Islets were suspended in PIM(T) media (Prodo Laboratory) upon arrival and immediately transferred into encapsulation device. MIN6 cells were obtained from American Type Culture Collection (ATCC), Manassas, VA. The cells were plated in T-75 flasks and cultured with Dulbecco's modified eagle's medium (DMEM, ATCC 30–2002) supplemented with 15% fetal bovine serum (S11550, Atlanta Biologicals) and 2% penicillin–streptomycin (10,000 U/mL, Thermo Fisher Scientific). Cells from low passage number (<5) were used. All cell culture was maintained in a humidified incubator with 5% CO_2 at 37 °C.

Optimization of Cell Loading Capacity. To determine the optimal loading density for viability, SC-βCs were loaded into the CC at multiple densities of IEQs (20, 10, 5, and 2.5 IEQ/μL). The percentage of viable cells was measured by alamarBlue assay and normalized to SC-βCs in Spinner flask. MIN6 cells (1.5×10^4 cells/μL, assuming 1,500 cells = 1 IEQ) were embedded in alginate hydrogel, loaded into the device, and then cultured in DMEM under normoxic (21% O_2) or hypoxic (6% O_2) condition. For hypoxic condition group, the devices were placed in a multigas incubator (MCO-5M, Sanyo) with air condition of 6% O_2 and 5% CO_2 at 37 °C. Low-oxygen tension was maintained through the controlled supply of N2 gas to the incubator (46).

Device Fabrication. The design for the main structure of the ceMED was completed using graphical illustration software (CorelDRAW) and produced with laser cutter on cast acrylic sheet-poly(methyl methacrylate) (McMaster-Carr). Device is 3.2 mm thick, 10 mm in length for CC and EqC, and 20 mm in length in total (dual-EqC ceMED: 30 mm in length). CC is 150 μL in volume, and a cell-seeding port is located on one side. Acrylic skeleton is attached with bilayer PTFE membranes (inner layer: 0.2 μm pore size, and 85 μm thickness from Sterlitech; outer layer: 10 μm pore size, 80% porosity, and 85 μm thickness from Millipore Sigma) using acrylic solvent cement (Scigrip). A precarved gap in the center of ceMED houses the HF (modified polyethersulfone, MWCO 100 kDa, and inner diameter 0.6 mm from Repligen), which is secured to the acrylic skeleton by epoxy glue (Loctite), and a connector at the entry point helps to connect to the silicone tubing (Tygon formulation 3350, Saint Gobain Performance Plastics) and pump. Devices were sterilized by ethanol wetting and ultraviolet treatment for 2 h followed by sterile PBS washes. The SC-βCs, MIN6, and primary human islets were loaded into the ceMED, and the loading port was sealed with Dermabond (Johnson & Johnson).

In Vitro Glucose Equilibration. Devices with different lengths of EqC (5, 10, and 20 mm) were fabricated for in vitro testing of glucose equilibration. For static control group, an isolated CC was used. Empty ceMEDs without cell sample were connected with inflow and outflow silicone tubing and submerged into a 10-mL reservoir with 5 mM glucose dissolved in PBS. Inlet was continuously pumped with PBS at multiple flow rates (100, 250, 500, and 1,000 μL/h). Small aliquots from the outflow or directly from the CC were collected for glucose concentration measurement at various time points with the Amplex Red Glucose assay (Thermo Fisher Scientific). To test responses to glucose dynamic changes, a ceMED was first submerged in a reservoir with 5 mM glucose concentration dissolved in PBS. After complete equilibration and saturation, fluid in the CC was collected through the cell-loading port using a syringe with a 30-gauge needle and dispensed in a centrifuge tube. A step change in glucose was stimulated by immersing the ceMED in a 13-mM glucose concentration reservoir then back into a 5-mM reservoir. Fluid in the CC was collected at multiple time points and measured by Amplex Red Glucose assay (Thermo Fisher Scientific).

Optimization of Loading Capacity. Twofold serial dilutions of SC-βCs were performed to prepare cell densities of 20, 10, 5, and 2.5 IEQ/μL. SC-βCs were then loaded into Matrigel (growth factor reduced, Corning) or alginate hydrogel (Millipore Sigma) –embedded devices through the cell-loading port and incubated in culture medium at 37 °C and 5% CO_2 either with perfused flow through the HF (100 μL/h) or no flow. Devices in the flow-enhanced condition were infused with PBS (Millipore Sigma) through silicone tubing (Saint Gobain Performance Plastics) connected at the entry point. Around 2 d after seeding, viability of SC-βCs was measured using alamarBlue assay (Invitrogen) and normalized to control cells cultured in spinner flask at respective densities. After optimization of cell density, cells at 10 IEQ/μL (150 μL) were loaded into CC for further experiments in vitro.

Gene Expression Analysis. qRT-PCR analysis was performed under a previously published protocol (47). MIN6 and SC-βCs were loaded into sterilized ceMEDs at a density of 10 IEQ/μL (with 150 μL in a device). After culturing, the devices were extracted, and the PTFE membranes were removed to expose cell samples. Total RNA was retrieved with the RNeasy Mini kit (Qiagen), following manufacturer's instructions. The RNA concentrations were quantified by NanoDrop spectrophotometer (Thermo Fisher Scientific). Similar amounts of RNA contents from each sample were loaded for complementary DNA synthesis using QuantiTect reverse transcription kit (Qiagen), following manufacturer's instructions. qRT-PCR was performed with 7900 Fast Real-Time PCR System (Applied Biosystems). SYBR Green PCR master mix (Applied Biosystems) and the following QuantiTect Primer Assays (Qiagen), with respective Entrez Gene ID, were used with the following: mouse BCL2 (12043), human BCL2 (596), mouse BAX (12028), human BAX (581), mouse glyceraldehyde 3-phosphate dehydrogenase (GAPDH) (14433), and human GAPDH (2597). Target gene expression levels were analyzed by the comparative C_t method and represented as a relative comparison with the static control group after normalization to endogenous GAPDH content.

Immunocytochemistry and Immunohistochemistry Staining for Retrieved Devices. Retrieved devices were fixed by submersion in 4% paraformaldehyde (Electron Microscopy Sciences) for 30 min at 4 °C and washed twice in PBS. Devices were then put onto a platform for excision of the content in the CC using a surgical blade while keeping the samples frozen by surrounding dry ice. Excised samples were embedded in optimal cutting temperature compounds (Sakura Finetek), and the blocks were allowed to harden on dry ice before being processed for cryosection. Cryosectioned slides were blocked with 5% donkey serum (Jackson ImmunoResearch) for 30 min at 4 °C and washed twice in PBS. For devices used for in vitro study, the TUNEL assay (Invitrogen) was used to identify apoptotic cells following manufacturer's instructions. Cellular nuclei were backstained with Hoechst 33342 (Invitrogen). For devices extracted from in vivo studies, the slides were immersed in primary antibody mixture overnight at 4 °C. The following primary antibodies were used at the indicated dilution factor: mouse monoclonal anti–C-peptide (1:300, Cell Signaling Technology), rabbit monoclonal anti-glucagon (1:1,000, Abcam), goat polyclonal anti-somatostatin (1:500, Santa Cruz), rabbit polyclonal anti-ColI (1:500, Abcam), mouse monoclonal anti–SMC-α (1:500, Millipore Sigma), and mouse monoclonal anti-CD68 (1:500, Abcam). Samples were then washed twice in PBS and stained with secondary antibodies, prepared in block solution at 1:500 dilution factor, for 30 min at 4 °C, and then washed twice in PBS. The following secondary antibodies were used: donkey anti-rabbit Alexa Fluor-647 (Invitrogen), goat anti-mouse Alexa Fluor-488 (Invitrogen), and goat anti-mouse Alexa Fluor-405 (Invitrogen). Nuclear staining was performed with DAPI (Millipore Sigma).

GSIS. The analysis was conducted following previously described procedure (48). The ceMEDs were loaded 150 μL of MIN6 cells or SC-βCs at a seeding density with 3 million cells or 2,000 IEQ. For SC-βCs, the cells were extracted from rat subcutaneous space 14-d posttransplantation and then measured using GSIS analysis. After overnight culture, the devices were removed from culture media and starved in 1.5-mL 2.8 mM glucose (Millipore Sigma) solution for 2 h. The devices were then sequentially submerged in solutions of 2.8 mM glucose, 20 mM glucose, 2.8 mM glucose, and 30 mM KCl for either 30 or 60 min each. Small aliquots of the solutions (10 μL) were collected at each time point and insulin content was quantified by mouse insulin enzyme-linked immunosorbent assay (ELISA) (Mercodia) and human ultrasensitive insulin ELISA kit (ALPCO Diagnostics). Then, the cells were collected and dispersed with TryplE (15 min), stained them with Trypan blue, and the glucose content was normalized to the number of live cells.

In Vivo Glucose Equilibration. For in vivo testing of glucose equilibration across the exposed HF in ceMED, an isolated EqC was fabricated, sterilized, and implanted into nondiabetic Lewis rats under the protocol outlined above. The inlet was pumped with either 2 or 20 mM sterilized glucose solution (PBS) at multiple flow rates (250, 500, and 1,000 μL/h). The outflow exiting the subcutaneous space and tail vein blood was collected at various time points. Small aliquots extracted from the outflow samples were analyzed for glucose concentration with Amplex Red Glucose assay (Thermo Fisher Scientific). The blood glucose level was measured using a glucose meter (Accu-Chek, Roche Diabetes Care)

In Vivo Glucose Monitoring after Device Transplantation. Sterilized ceMEDs were loaded with primary human islets or MIN6 at 2,000 IEQ (3×10^6 cells) and transplanted into the subcutaneous space of animal recipients. For this study, immunocompetent Lewis rats were induced to become diabetic through a single IP injection of 60 mg/kg STZ suspended in 100 mM sodium citrate buffer (pH 4.5). After 3-d postinduction, a blood sample was collected from the tail veins of the injected rats to measure blood glucose. The rats were selected for transplantation after the results came back at >300 mg/dL blood glucose at least 3 to ∼4 measurements to ensure they were diabetic (glucose meter, Accu-Chek).

IPGTT. At day 14, IPGTT was performed. The rats were starved for 12 h and then injected with 2 g/kg glucose suspended in PBS through IP. Tail vein blood was collected just prior to injection and at various time points after injection for reading with glucose meter (Accu-Chek). The human insulin level was measured using collected blood by human insulin ELISA kits (Alpco) until device extraction.

Retrieval of ceMED and Processing. Devices were retrieved after 14 d on the basis of other transplantation experiments and fibrotic encapsulation studies (44, 49). After the animals were killed with CO_2, the devices were extracted from the dorsal subcutaneous space and washed twice in PBS. Retrieved devices were fixed, cryosectioned, and processed for histological sectioning. Histological sections were then stained with hematoxylin and eosin (H&E) and Masson's trichrome staining at the Koch Institute at Massachusetts Institute of Technology or processed for immunohistochemical imaging. Quantification of thickness of fibrosis was performed on H&E-stained sections using ImageJ software (NIH). To visualize potential angiogenesis, the surface of device was stained with 3,3′-diaminobenzidine with horseradish peroxidase substrate (Invitrogen) and imaged with a bright-field microscope. To retrieve the encapsulated cells for insulin secretion test, the devices were washed with PBS thoroughly and the PTFE membrane on one side of the CC was lifted off using a tweezer. The enclosed cells were extracted and transferred to a well plate. The cells were tested for insulin secretion following 14 d by ELISA kit (R&D systems). The GSIS was performed as previously described in the GSIS section. For immunofluorescent staining of endocrine markers (C-peptide, glucagon, and somatostatin), cells were extracted from the CC following 7-d post-transplantation, and staining was performed as described in the *Immunocytochemistry and Immunohistochemistry Staining* section.

Statistical Analysis. All experimental data were analyzed with GraphPad Prism version 8 (GraphPad Software). Values were presented as mean ± SD and assessed for statistical significance using one-way or two-way ANOVA followed by multiple comparison tests (Dunnett's or Tukey's) where * indicates $P < 0.05$, ** indicates $P < 0.01$, and *** indicates $P < 0.001$. The displayed in vitro data were collected from at least three biological replicates. In vivo validation was also collected from 2 to ∼3 biological replicates. When comparisons with multiple groups were made, additional symbols were used. The number of replicates was indicated under the figure captions for each graph.

Data Availability. All study data are included in the article and/or *SI Appendix*.

ACKNOWLEDGMENTS. This work was supported by the NIH through R01 Grant HL095722 and the JDRF (Grant 3-SRA-2013-282) to J.M.K. and Grant U01DK104218 (NIH) to D.L.G. This work was also supported by the Incheon National University Research Grant in 2021 to K.Y.

1. W.-P. You, M. Henneberg, Type 1 diabetes prevalence increasing globally and regionally: The role of natural selection and life expectancy at birth. *BMJ Open Diabetes Res. Care* **4**, e000161 (2016).
2. A. M. J. Shapiro, M. Pokrywczynska, C. Ricordi, Clinical pancreatic islet transplantation. *Nat. Rev. Endocrinol.* **13**, 268–277 (2017).
3. E. A. Ryan *et al.*, Clinical outcomes and insulin secretion after islet transplantation with the Edmonton protocol. *Diabetes* **50**, 710–719 (2001).
4. A. M. J. Shapiro *et al.*, International trial of the Edmonton protocol for islet transplantation. *N. Engl. J. Med.* **355**, 1318–1330 (2006).
5. A. M. J. Shapiro *et al.*, Islet transplantation in seven patients with type 1 diabetes mellitus using a glucocorticoid-free immunosuppressive regimen. *N. Engl. J. Med.* **343**, 230–238 (2000).
6. B. Ritz-Laser *et al.*, Molecular detection of circulating β-cells after islet transplantation. *Diabetes* **51**, 557–561 (2002).
7. A. M. Davalli *et al.*, A selective decrease in the beta cell mass of human islets transplanted into diabetic nude mice. *Transplantation* **59**, 817–820 (1995).
8. E. A. Ryan *et al.*, Five-year follow-up after clinical islet transplantation. *Diabetes* **54**, 2060–2069 (2005).

9. J. Dantal, J.-P. Soulillou, Immunosuppressive drugs and the risk of cancer after organ transplantation. *N. Engl. J. Med.* **352**, 1371–1373 (2005).
10. T. Desai, L. D. Shea, Advances in islet encapsulation technologies. *Nat. Rev. Drug Discov.* **16**, 338–350 (2017). Correction in: *Nat. Rev. Drug Discov.* **16**, 367 (2017).
11. F. W. Pagliuca *et al*., Generation of functional human pancreatic β cells in vitro. *Cell* **159**, 428–439 (2014).
12. T. Boettler *et al*., Pancreatic tissue transplanted in TheraCyte encapsulation devices is protected and prevents hyperglycemia in a mouse model of immune-mediated diabetes. *Cell Transplant.* **25**, 609–614 (2016).
13. P.-O. Carlsson *et al*., Transplantation of macroencapsulated human islets within the bioartificial pancreas βAir to patients with type 1 diabetes mellitus. *Am. J. Transplant.* **18**, 1735–1744 (2018).
14. T. Robert *et al*., Functional beta cell mass from device-encapsulated hESC-derived pancreatic endoderm achieving metabolic control. *Stem Cell Reports* **10**, 739–750 (2018).
15. N. Trivedi, G. M. Steil, C. K. Colton, S. Bonner-Weir, G. C. Weir, Improved vascularization of planar membrane diffusion devices following continuous infusion of vascular endothelial growth factor. *Cell Transplant.* **9**, 115–124 (2000).
16. M. D. Menger, P. Vajkoczy, C. Beger, K. Messmer, Orientation of microvascular blood flow in pancreatic islet isografts. *J. Clin. Invest.* **93**, 2280–2285 (1994).
17. G. Faleo, K. Lee, V. Nguyen, Q. Tang, Assessment of immune isolation of allogeneic mouse pancreatic progenitor cells by a macroencapsulation device. *Transplantation* **100**, 1211–1218 (2016).
18. E. Rafael, G. S. Wu, K. Hultenby, A. Tibell, A. Wernerson, Improved survival of macroencapsulated islets of Langerhans by preimplantation of the immunoisolating device: A morphometric study. *Cell Transplant.* **12**, 407–412 (2003).
19. M. Kumagai-Braesch *et al*., The TheraCyte™ device protects against islet allograft rejection in immunized hosts. *Cell Transplant.* **22**, 1137–1146 (2013).
20. K. Wang *et al*., The paracrine effects of adipose-derived stem cells on neovascularization and biocompatibility of a macroencapsulation device. *Acta Biomater.* **15**, 65–76 (2015).
21. G. Orlando *et al*., Cell replacement strategies aimed at reconstitution of the β-cell compartment in type 1 diabetes. *Diabetes* **63**, 1433–1444 (2014).
22. T. Neufeld *et al*., The efficacy of an immunoisolating membrane system for islet xenotransplantation in minipigs. *PLoS One* **8**, e70150 (2013).
23. P. de Vos, P. Marchetti, Encapsulation of pancreatic islets for transplantation in diabetes: The untouchable islets. *Trends Mol. Med.* **8**, 363–366 (2002).
24. R. Chang *et al*., Nanoporous immunoprotective device for stem-cell-derived β-cell replacement therapy. *ACS Nano* **11**, 7747–7757 (2017).
25. A. Rodriguez-Brotons *et al*., Impact of pancreatic rat islet density on cell survival during hypoxia. *J. Diabetes Res.* **2016**, 3615286 (2016).
26. S. Song, S. Roy, Progress and challenges in macroencapsulation approaches for type 1 diabetes (T1D) treatment: Cells, biomaterials, and devices. *Biotechnol. Bioeng.* **113**, 1381–1402 (2016).
27. E. C. Heher, T. R. Spitzer, N. B. Goes, Light chains: Heavy burden in kidney transplantation. *Transplantation* **87**, 947–952 (2009).
28. S. Genuth *et al*.; Expert Committee on the Diagnosis and Classification of Diabetes Mellitus, Follow-up report on the diagnosis of diabetes mellitus. *Diabetes Care* **26**, 3160–3167 (2003).
29. A. Tirosh *et al*.; Israeli Diabetes Research Group, Normal fasting plasma glucose levels and type 2 diabetes in young men. *N. Engl. J. Med.* **353**, 1454–1462 (2005). Correction in: *N. Engl. J. Med.* **354**, 2401 (2006).
30. T. P. Vahl *et al*., Meal feeding improves oral glucose tolerance in male rats and causes adaptations in postprandial islet hormone secretion that are independent of plasma incretins or glycemia. *Am. J. Physiol. Endocrinol. Metab.* **307**, E784–E792 (2014).
31. H. Ishihara *et al*., Pancreatic beta cell line MIN6 exhibits characteristics of glucose metabolism and glucose-stimulated insulin secretion similar to those of normal islets. *Diabetologia* **36**, 1139–1145 (1993).
32. W. Zhang *et al*., Neuromedin U suppresses glucose-stimulated insulin secretion in pancreatic β cells. *Biochem. Biophys. Res. Commun.* **493**, 677–683 (2017).
33. D. Johnson *et al*., Glucose-dependent modulation of insulin secretion and intracellular calcium ions by GKA50, a glucokinase activator. *Diabetes* **56**, 1694–1702 (2007).
34. A. J. Vegas *et al*., Long-term glycemic control using polymer-encapsulated human stem cell-derived beta cells in immune-competent mice. *Nat. Med.* **22**, 306–311 (2016).
35. Y. Sato, M. Inoue, T. Yoshizawa, K. Yamagata, Moderate hypoxia induces β-cell dysfunction with HIF-1-independent gene expression changes. *PLoS One* **9**, e114868 (2014).
36. J. Weidling, S. Sameni, J. R. T. Lakey, E. Botvinick, Method measuring oxygen tension and transport within subcutaneous devices. *J. Biomed. Opt.* **19**, 087006 (2014).
37. S.-H. Lee *et al*., Human beta-cell precursors mature into functional insulin-producing cells in an immunoisolation device: Implications for diabetes cell therapies. *Transplantation* **87**, 983–991 (2009).
38. M. Qi *et al*., PVA hydrogel sheet macroencapsulation for the bioartificial pancreas. *Biomaterials* **25**, 5885–5892 (2004).
39. S. Merani, C. Toso, J. Emamaullee, A. M. J. Shapiro, Optimal implantation site for pancreatic islet transplantation. *Br. J. Surg.* **95**, 1449–1461 (2008).
40. V. A. Bolaños Quiñones, H. Zhu, A. A. Solovev, Y. Mei, D. H. Gracias, Origami biosystems: 3D assembly methods for biomedical applications. *Adv. Biosyst.* **2** (2018).
41. J. M. Anderson, A. Rodriguez, D. T. Chang, Foreign body reaction to biomaterials. *Semin. Immunol.* **20**, 86–100 (2008).
42. R. C. Taylor, S. P. Cullen, S. J. Martin, Apoptosis: Controlled demolition at the cellular level. *Nat. Rev. Mol. Cell Biol.* **9**, 231–241 (2008).
43. H. Kono, K. L. Rock, How dying cells alert the immune system to danger. *Nat. Rev. Immunol.* **8**, 279–289 (2008).
44. E. B. Dolan *et al*., An actuatable soft reservoir modulates host foreign body response. *Sci. Robot.* **4**, eaax7043 (2019).
45. S. Farah *et al*., Long-term implant fibrosis prevention in rodents and non-human primates using crystallized drug formulations. *Nat. Mater.* **18**, 892–904 (2019).
46. K. Yang *et al*., A microfluidic array for quantitative analysis of human neural stem cell self-renewal and differentiation in three-dimensional hypoxic microenvironment. *Biomaterials* **34**, 6607–6614 (2013).
47. K. Yang *et al*., Electroconductive nanoscale topography for enhanced neuronal differentiation and electrophysiological maturation of human neural stem cells. *Nanoscale* **9**, 18737–18752 (2017).
48. K. Yang *et al*., A 3D culture platform enables development of zinc-binding prodrugs for targeted proliferation of β cells. *Sci. Adv.* **6**, eabc3207 (2020).
49. O. Veiseh *et al*., Size- and shape-dependent foreign body immune response to materials implanted in rodents and non-human primates. *Nat. Mater.* **14**, 643–651 (2015).